CHAPTER III

RESULTS

In this chapter, we present and discuss the results which are divided in 3 parts: characterization part, drag reduction part and scaling analysis part.

3.1 Characterizations

3.1.1 Polyacrylamide

3.1.1.1 Static Light Scattering Static light scattering measurements were carried out to determine the weight average molecular weights, M_w and the radii of gyration, R_g of the polymers used in this study.

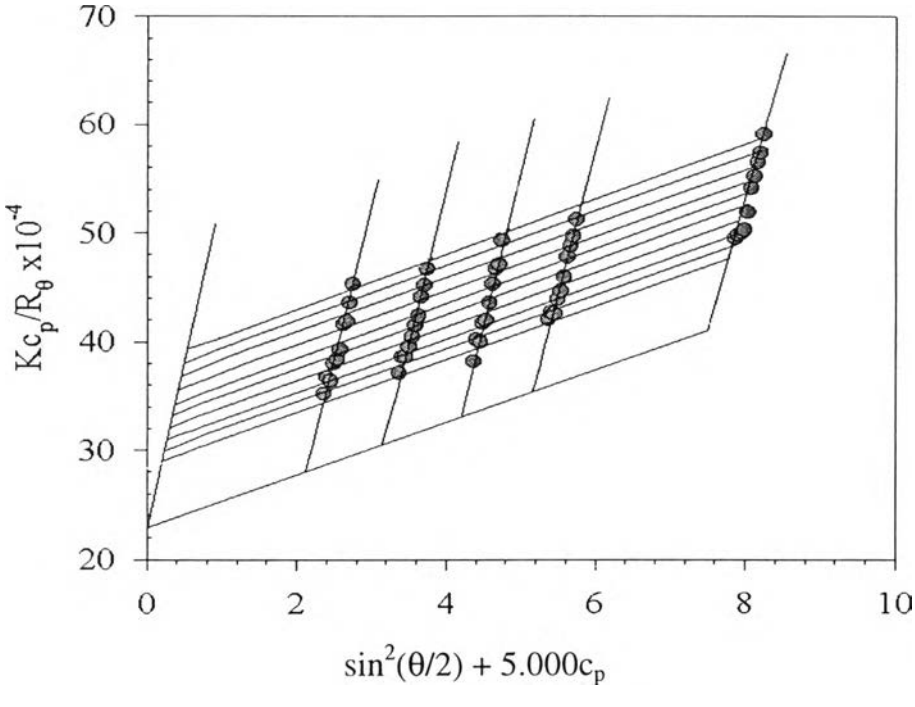

Figure 3.1 (a) Zimm plot for light scattering intensity of PAM-PS-19901 solutions at 30°C.

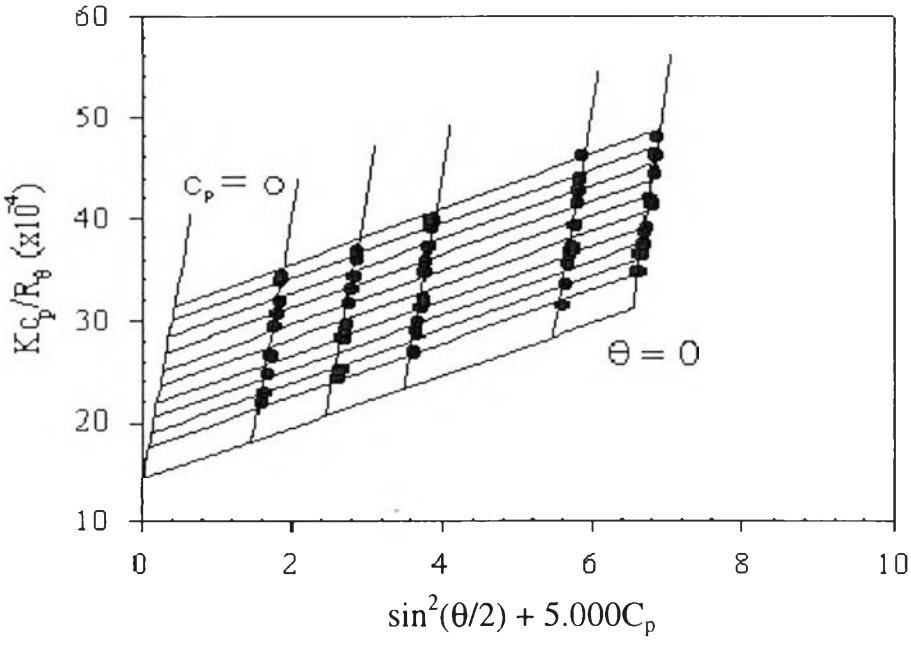

Figure 3.1(b) Zimm plot for light scattering intensity of PAM-PS-02806 solutions at 30°C.

Figures 3.1 (a) and (b) show a typical Zimm plot of the polyacrylamides in water, where polymer concentration was varied from 0.2 to 1.5 g/l at 30°C. The differential refractive indices increment (dn/dc_p) for the polyacrylamides in water are listed in Table 2.3. On the basis of equation 2.1, M_w, A_2 and R_g were determined from the extrapolations of $[Kc_p/R_\theta]_{q\to0,\ c\to0}$, $[Kc_p/R_\theta]_{c\to0}$ versus q^2 and $[Kc_p/R_\theta]_{q\to0}$ versus c_p, respectively. The results are tabulated in Table 3.1. The positive values of the second virial coefficient, A_2 show that water is a reasonably good solvent. A_2 seems to decrease slightly with increasing molecular weight, in agreement with the result of Munk et al. (1980), Patterson and Jamieson (1985).

3.1.1.2 Dynamic Light Scatstering. Dynamic light scattering measurements were carried out to determine polymer solution properties.

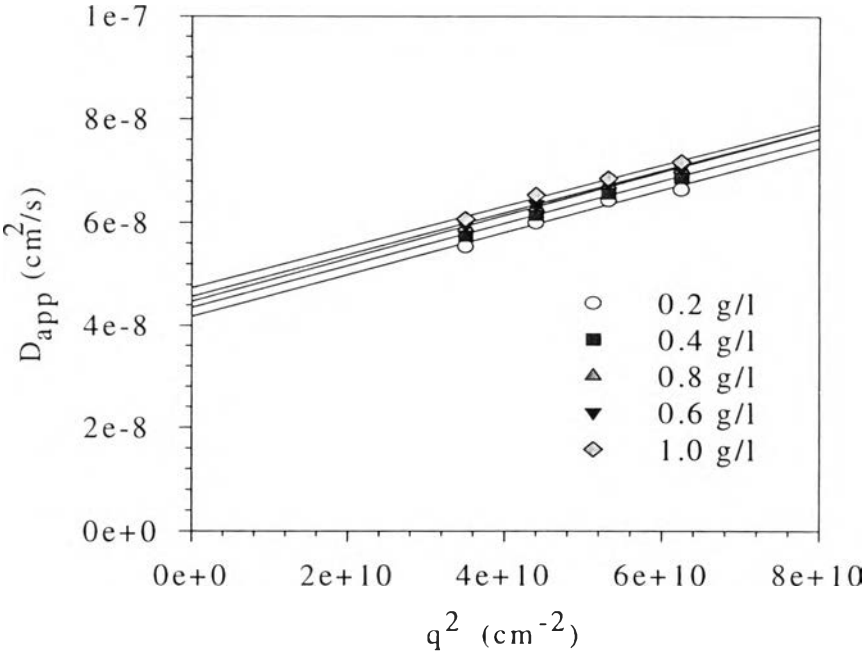

Figure 3.2 (a) Apparent diffusion coefficient as a function of the square of scattering wave vector for PAM-PS-02806 solutions at 30°C.

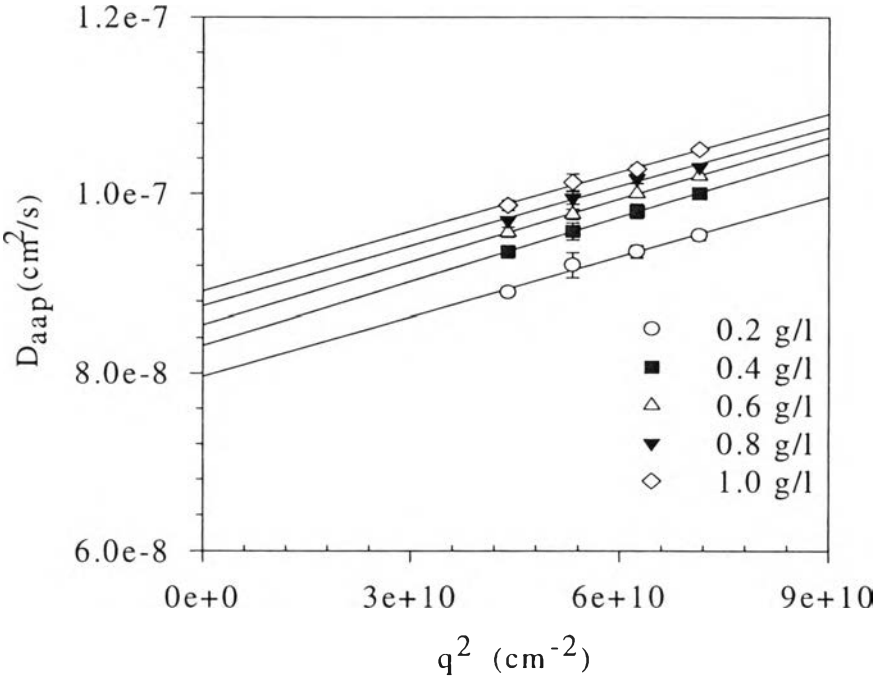

Figure 3.2 (b) Apparent diffusion coefficient as a function of the square of scattering wave vector for PAM-PS-19901 solutions at 30°C.

Table 3.1 Static light scattering properties of polyacrylamide solutions at 30°C.

Sample	$M_w x 10^{-6}$(g/mol)	R_g (nm)	A_2 (cm^2/ (g^2/mol))
PS-19901	0.52	62.6	0.00124
PS-02806	2.15	150.2	0.00100
Munk et al.	0.26	-	0.00032
Munk et al.	2.10	-	0.00027
Patterson and Jamieson	0.48	-	0.00037
Patterson and Jamieson	5.26	151.0	0.00025

Plots of apparent diffusion coefficient versus scattering wave vector square, q^2, with θ ranging from 80 to 110 at 30°C are shown in figures 3.2 (a) and (b) as a function of polymer concentration. Linear lines can

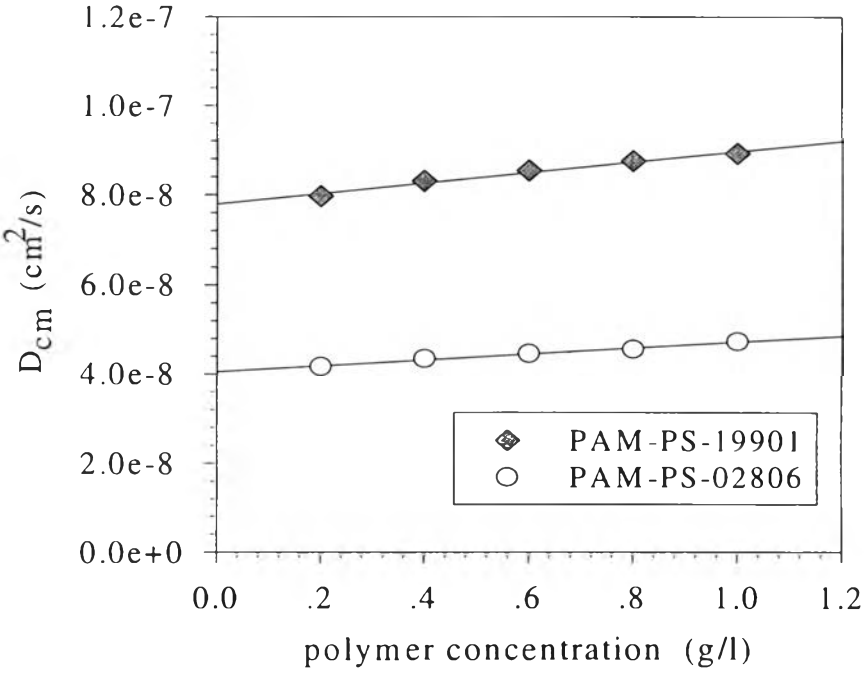

Figure 3.3 Center of mass diffusion coefficient versus polymer concentration for PAM-PS-19901 and PAM-PS-02806 solutions at 30°C.

be drawn through data points. On the basis of equation 2.10, the center of mass diffusion coefficient was obtained from the intercept of each polymer concentration.

Figure 3.3 shows the concentration dependence of the center of mass diffusion coefficient at 30°C. All data points follow a linear dependence as in equation 2.11. From the intercept of these lines, the diffusion coefficient of infinite dilution, D_o were obtained and then converted to the hydrodynamic radius, R_h by using the Stoke-Einstein equation (equation 2.12). R_h of PAM-PS-19901 and PAM-PS-02806 are 35.6 and 68.4 nm, respectively. Dynamic properties are tabulated in Table 3.3.

Figure 3.4 shows polydispersity of relaxation time of polyacrylamide solutions, μ_2/Γ^2, versus polymer concentration at the scattering angle of 90°. The polydispersity increases linearly with polymer concentration. The polydispersity of polyacrylamide-PS-02806 and PS-19901 at infinite dilution are 0.437 and 0.309, respectively.

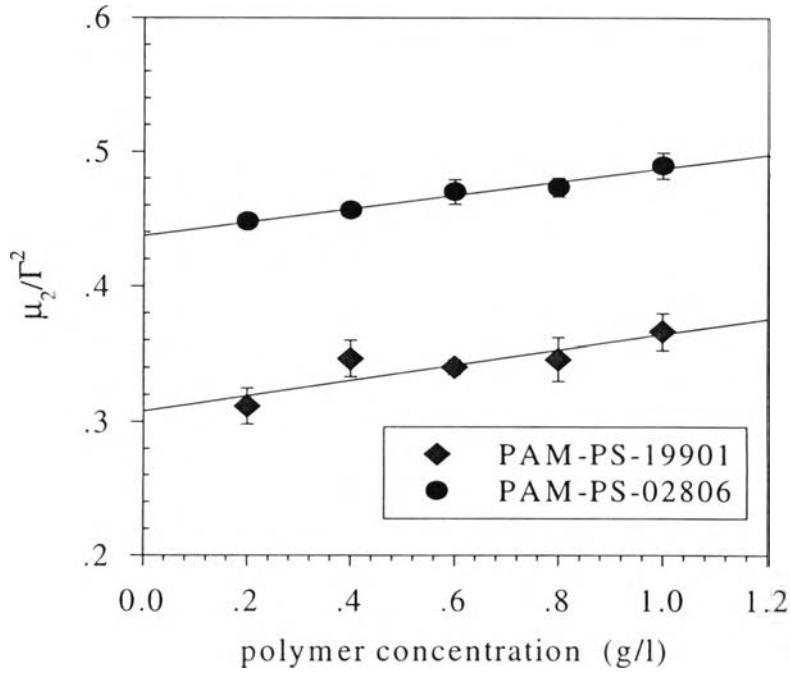

Figure 3.4 Polydispersity of relaxation time of polyacrylamide solutions at scattering angle of 90° as a function of polymer concentration at 30°C.

3.1.1.3 Viscosity. Figures 3.5 (a), (b) and (c) show reduced viscosity, η_{sp}/c_p as a function of polymer concentration for PAM-PS-22581, PAM-PS-19901, PAM-PS-02806 and PAM-PS-18522 solutions at 30°C. The plot yields the intrinsic viscosity from the intercept and the Huggins constant from the slope of the linearly fitted line through the experimental points according to the Huggins equation (equation 2.16). The intrinsic viscosities and Huggins constants of the samples are tabulated in Table 3.3 together with values of viscosity average molecular weight, M_v, obtained by using the Houwink-Mark-Sakurada equation (equation 2.17). In this work, we used the relation:

$$[\eta] = 6.5 \times 10^{-6} M_v^{\,0.82}. \qquad (3.1)$$

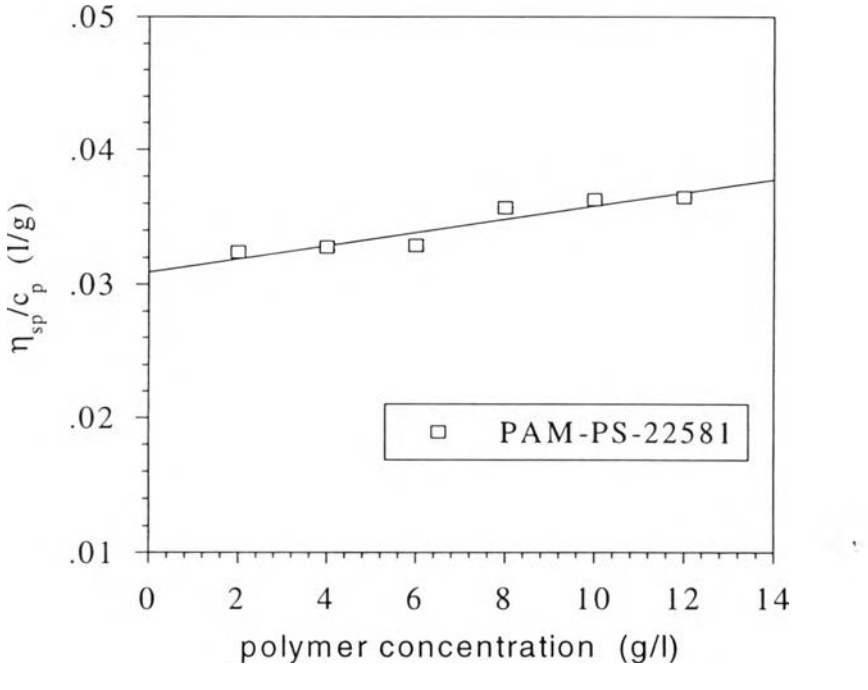

Figure 3.5 (a) Reduced viscosity as a function of polymer concentration at 30°C for PAM-PS-22581 in 0.1 M NaCl.

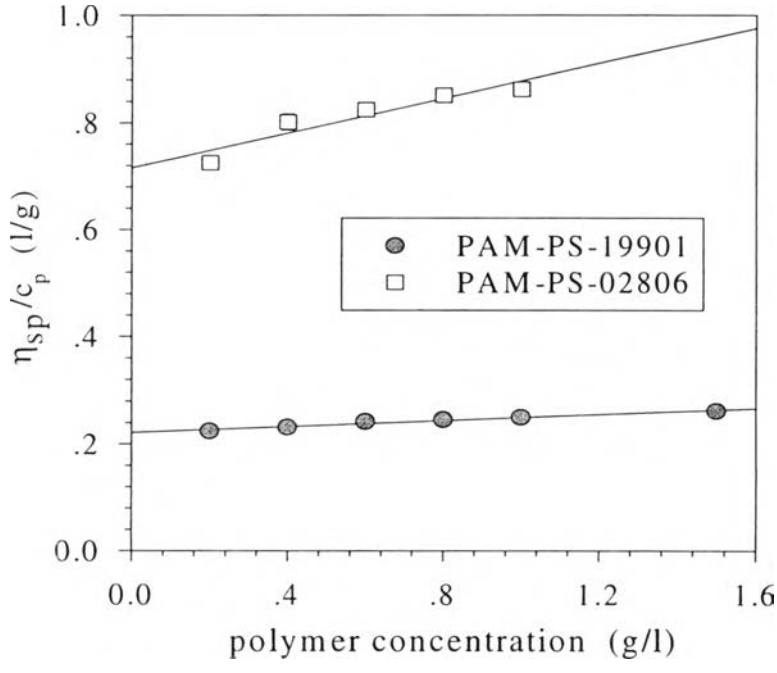

Figure 3.5 (b) Reduced viscosity as a function of polymer concentration at 30°C for PAM-PS-19901and PAM-PS-02806 in water.

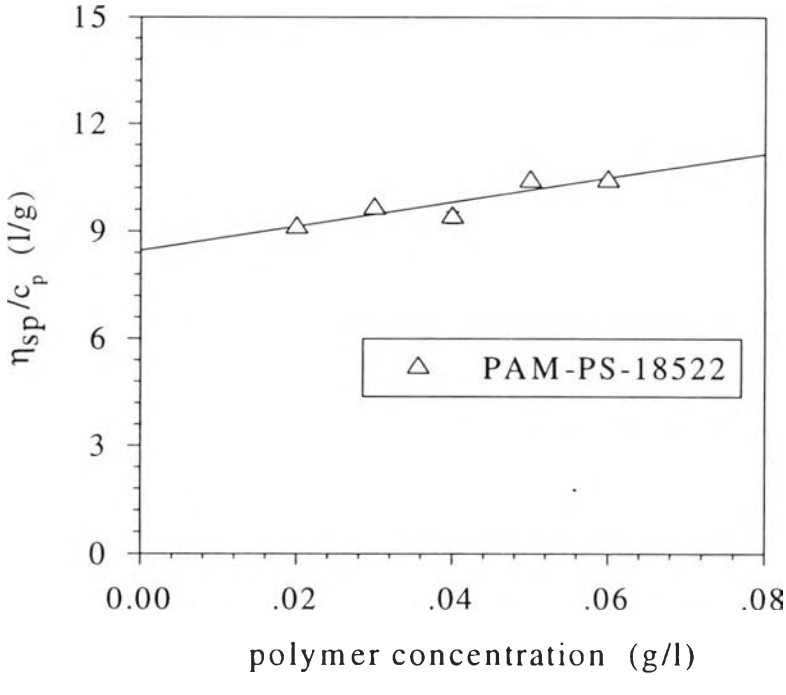

Figure 3.5 (c) Reduced viscosity as a function of polymer concentration at 30°C for PAM-PS-19901and PAM-PS-02806 in water.

In Table 3.3, the Huggins constants, k_H, which represent the interaction between water and PAM-(PS-19901, PS-02806, PS-18522) and interaction between PAM-PS-22581and 0.1 M NaCl vary between 0.3-0.5. The value of k_H is often near 0.35 for flexible polymer molecules in good solvent (Kadi and Carreau, 1987). Thus, water is a good solvent for PAM-(PS-19901, PS-02806, PS-18522) while 0.1 M NaCl is also a good solvent for PAM-PS-22581.

Another quantity of particular interest is the overlap concentration, C_p^* defined by:

$$C_p^*[\eta]=1. \tag{3.2}$$

The values of C_p^* are tabulated in Table 3.2. C_p^* is approximately the polymer concentration at which chains overlap and the solution becomes semidilute.

Table 3.2 Overlap concentration of polyacrylamide at 30°C.

Sample	[η] l/g	C_p^* (g/l)
PS-22581 in 0.1 M NaCl	0.031 ± 0.001	32.3 ± 1.0
PS-19901 in water	0.221 ± 0.002	4.52 ± 0.04
PS-02806 in water	0.72 ± 0.02	1.39 ± 0.04
PS-18522 in water	8.24 ± 0.75	0.12 ± 0.01

Table 3.3 Dynamic light scattering properties of PAM solutions at 30°C.

Sample	22581[a]	19901	02806	18522
$D_o x10^8$ (cm^2/s)	-	7.79 ± 0.06	4.06 ± 0.03	-
R_h (nm)	-	35.6 ± 0.3	68.4 ± 0.5	-
D_{cm}[b] $x10^8$ (cm^2/s)	-	7.91 ± 0.07	4.12 ± 0.03	1.25 ± 0.14
R_h[c] (nm)	-	35.1 ± 0.3	67.3 ± 0.5	222 ± 25
μ_2/Γ^2	-	0.309 ± 0.007	0.437 ± 0.009	-
[η] (l/g)	0.031±0.001	0.221 ± 0.002	0.72 ± 0.02	8.24 ± 0.75
k_H	0.52 ±0.11	0.56 ± 0.05	0.32 ± 0.07	0.47 ± 0.13
M_v $x10^{-5}$(g/mol)	-	5.45 ± 0.05	29.9 ± 0.7	107 ± 4
M_w $x10^{-5}$(g/mol)	-	4.95	21.5	-
M_w[d] (g/mol)	10,000	700,000	5,000,000	18,000,000

[a] PAM-PS-22581 in 0.1 M NaCl

PAM-19901, PAM-PS-02806 and PAM-PS-18522 in water

[b, c] at 100 mg/l

[d] quoted by supplier

3.1.2 70% Hydrolyzed Polyacrylamide

3.1.2.1 Static Light Scattering. Figure 3.6 shows a Zimm plot of 70% hydrolyzed polyacrylamide–SPP-377 in 0.02 M NaCl where polymer concentrations were varied from 0.2 to 0.8 g/l at 30°C. The differential refractive index increment was determined and found to be 0.167 (Table 2.3). From equation 2.5, the molecular weight was obtained from the inverse of the intercept of lines $c_p = 0$ and $\theta = 0$ in the Zimm plot. The slope of the zero concentration line as a function of angle provided a measure of R_g. The results are tabulated in Table 3.4.

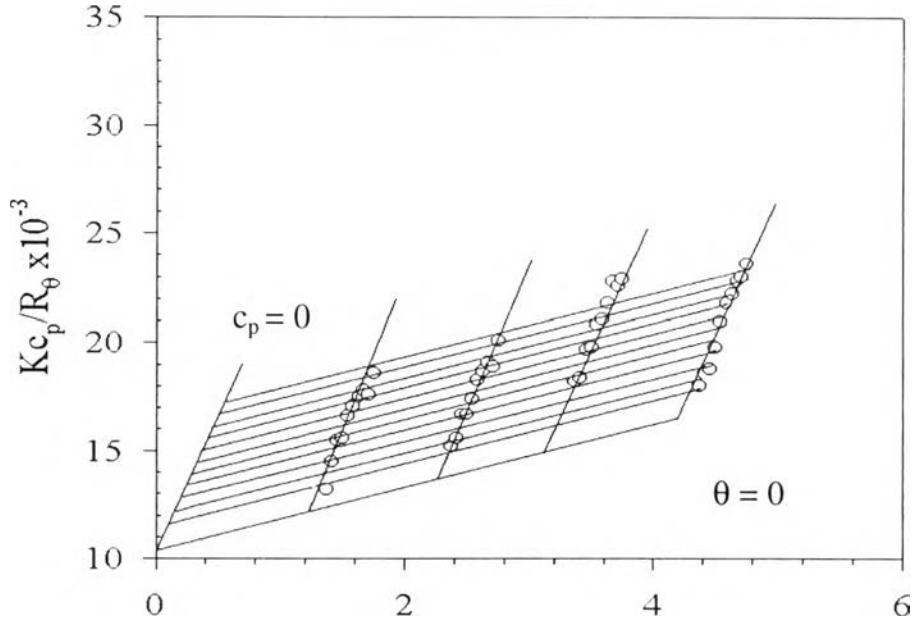

Figure 3.6 Zimm plot for light scattering intensity of 70%HPAM-SPP-377 in 0.02 M NaCl solutions at 30°C.

Table 3.4 Static light scattering properties of 70% hydrolyzed polyacrylamide in 0.02 M NaCl at 30°C.

Sample	M_w (g/mol)	R_g (nm)	A_2
70 % HPAM-SPP-377	178000	78.0	0.0156

3.1.2.2 Dynamic Light Scattering. Figure 3.7 shows the plots of apparent diffusion coefficient, D_{app}, for 100 ppm of 70% hydrolyzed polyacrylamide at various NaCl concentrations as a function of scattering wave vector square, q^2 at 30°C. D_{app} has a linear dependence on q^2 according to equation 2.10. The linear line can be drawn through data points. The center of mass diffusion coefficients obtained from the intercept were converted to the hydrodynamic radius, R_h, by using the Stoke-Einstein equation (equation 2.12). R_h of 70% hydrolyzed polyacrylamide are tabulated in Table 3.5.

As demonstrated in Table 3.5, 70% hydrolyzed polyacrylamide solutions display a larger R_h in aqueous than in saline solutions. In water, the chain expands due to strong intramolecular-ionic bonding. When salt is added, the charges on the polymer chain are partially shielded by the electrolyte and the chain collapes. When salt concentration is further increased to 0.5 M NaCl, R_h does not decrease significantly below the lower value. This is because of the rigidity of the chain.

3.1.2.3 Viscosity. Figure 3.8 shows reduced viscosity as a function of polymer concentration of 70% hydrolyzed polyacrylamide solutions at 30°C. In aqueous solution, the reduced viscosity of this polyelectrolyte shows a strong upward curvature rather than linear extrapolations of η_{sp}/c_p to zero polymer concentration. This data can be fitted by the Fuoss and Strauss equation:

Table 3.5 Dynamic light scattering properties of 100 mg/l 70% hydrolyzed polyacrylamide in various salt concentrations at 30°C.

NaCl (M)	D_{cm} x10^8 (cm^2/s)	R_h (nm)
0	1.07 ± 0.17	259 ± 41
0.005	2.59 ± 0.32	107 ± 13
0.01	2.97 ± 0.45	93 ± 14
0.02	3.33 ± 0.42	83 ± 11
0.05	3.45 ± 0.30	80 ± 7
0.1	3.75 ± 0.26	74 ± 5
0.2	4.48 ± 0.23	62 ± 3
0.5	4.62 ± 0.45	60 ± 6

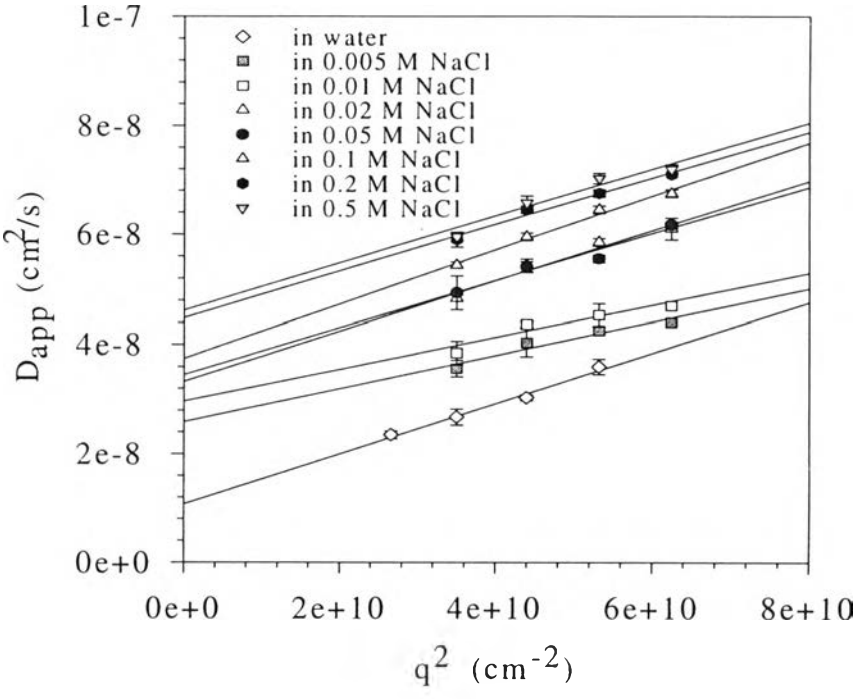

Figure 3.7 Apparent diffusion coefficient as a function of the square of scattering wave vector at 30°C for 70% HPAM-SPP-377 at various polymer concentrations.

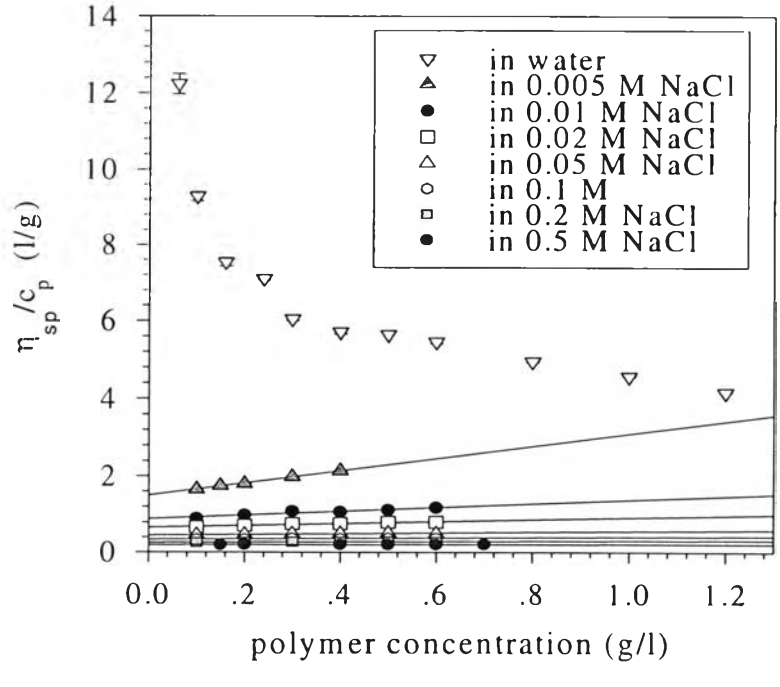

Figure 3.8 Reduced viscosity as a function of polymer concentration at 30°C for 100 mg/l 70%HPAM-SPP-377 in sterile water and various salt concentrations.

$$\frac{\eta_{sp}}{c_p} = \frac{[\eta]}{1 + B\sqrt{c_p}}, \tag{3.3}$$

where $Bc_p^{1/2}$ provides interaction between polyions and coions (Fuoss and Strauss, 1948). However, upon the addition of salts (NaCl), the unbounded rise is replaced by a simple linear extrapolation to zero polymer concentration, which can be fitted by the Huggins equation (equation 2.16). This effect is due to the decrease in ionic strength of the solution when a polyelectrolyte is diluted. The decrease in ionic-strength of the solution as concentration decreases results in an increase in the Debye length which is the distance over which electrostatic interactions can be manifested, resulting in changes in the hydrodynamic interaction of polyelectrolyte and solvent and increases in intermolecular interactions and chain expansion.

The data of [η] and k_H are tabulated in Table 3.6. The intrinsic viscosity, [η] was found to decrease with the amount of added salt. These values are of the same order of magnitude as those obtained by Kadi and Carreau (1987).

The Huggin coefficients, k_H, obtained from the slope of the straight line of η_{sp}/c_p versus c_p decreases from 0.73 at 0.005 M NaCl to 0.39 at 0.5 M NaCl. The large value of k_H observed at low salt concentration (low ionic strengths) is thought to arise from strong intermolecular interaction, while the value at the highest ionic strength suggests a theta state chain.

The value of C_p^* were found to increase with salt concentrations, indicating that overlapping of smaller hydrodynamic volume chains occurs at higher polymer concentrations. Clearly, the hydrodynamic interaction depends on the ionic strength of the solution.

Table 3.6 Intrinsic viscosity, Huggins coefficient and overlap concentration of 70% hydrolyzed polyacrylamide at various salt concentrations at 30°C.

NaCl (M)	[η] (l/g)	C_p^* (g/l)	k_H
0	-	-	-
0.005	1.49 ± 0.04	0.67 ± 0.02	0.73 ± 0.02
0.01	0.88 ± 0.03	1.14 ± 0.04	0.65 ± 0.02
0.02	0.66 ± 0.02	1.52 ± 0.03	0.59 ± 0.01
0.05	0.45 ± 0.01	2.22 ± 0.06	0.57 ± 0.01
0.10	0.34 ± 0.01	2.94 ± 0.05	0.53 ± 0.01
0.2	0.26 ± 0.01	3.85 ± 0.11	0.46 ± 0.01
0.5	0.19 ± 0.01	5.26 ± 0.13	0.39 ± 0.02

3.2 Drag Reduction Measurement

Figures 3.9 (a), (b) and (c) show a plot of friction factor versus Reynolds number for water/glycerol mixtures at the ratios of 100/0 and 70/30 at 30°C. Taylor instabilities transition and turbulent transition occur at Reynolds numbers of about 60 and 1000, respectively. Walowit et al. (1964) found Taylor instabilities transition and turbulent transition occurred at Reynolds numbers of 68 and 1600 in a Couette device with nearly the same geometry. The critical Re for Taylor instabilities compared well with those obtained from Walowit et al.. The lower turbulent transition Re may come from several factors: one being the surface roughness of the plexiglas used.

3.2.1 Effect of Polymer Concentration. The effect of polymer concentration was studied by using polymer samples with a fixed molecular weight and identical chemical structures but at different polymer concentrations.

Figure 3.10 is a plot of friction factor versus Reynolds number for PAM-PS-02806 solutions measured in our homemade Couette apparatus at 30°C. As the molecular weight is held constant, friction factor decreases with increasing polymer concentrations. % Turbulent drag reduction is calculated by:

$$\% \text{ turbulent drag reduction} = \frac{f_o - f}{f_o} \times 100, \tag{3.4}$$

where f_o is friction factor of solvent (water) and f is friction factor of solution.

Figure 3.11 shows % turbulent drag reduction versus polymer concentration of PAM-PS-02806 and PS-19901 solutions at Reynolds number of 5460 at 30°C. As expected, % turbulent drag reduction initially increases with

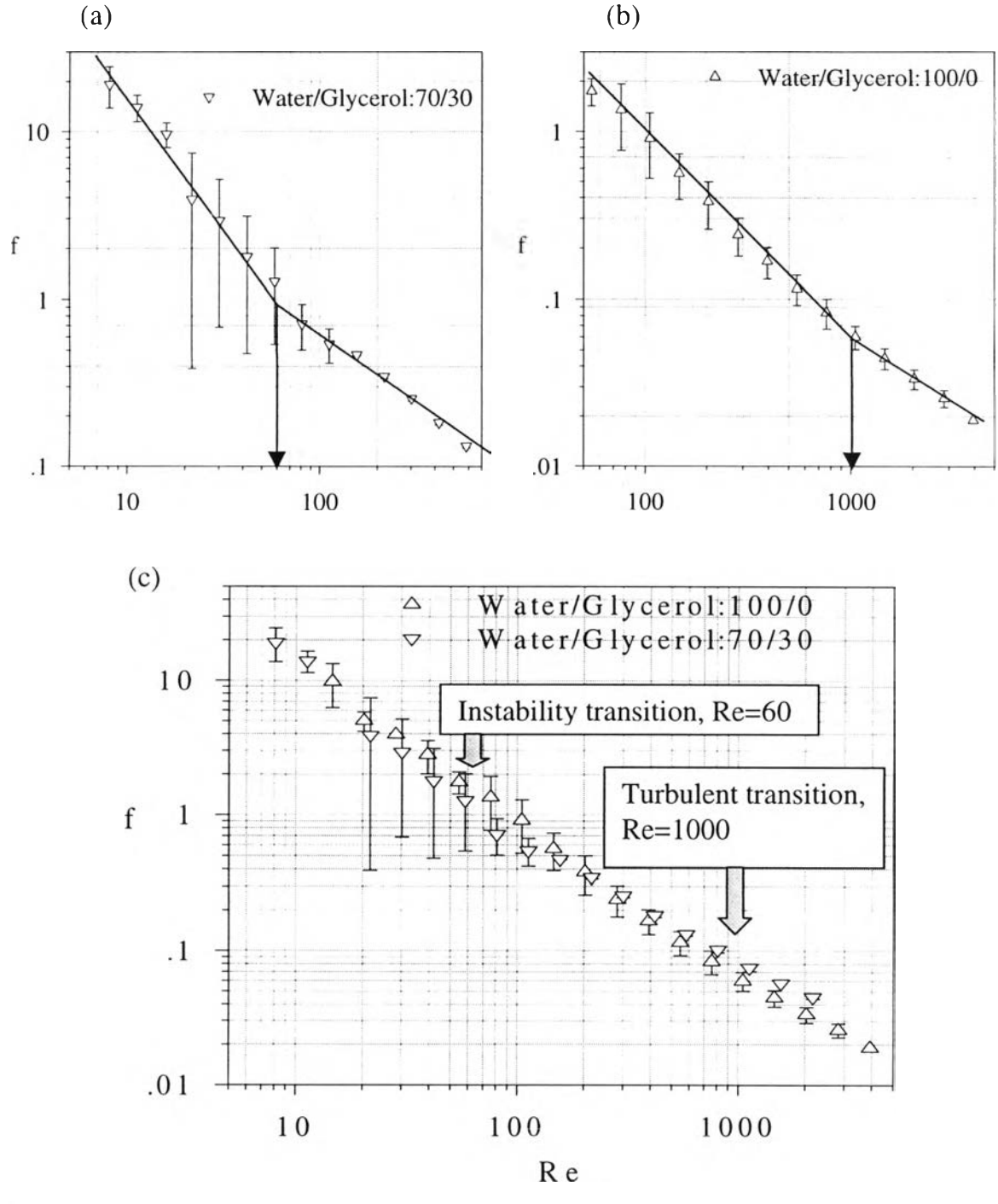

Figure 3.9 Friction factor versus Reynolds number for: (a) water/glycerol: 70/30 mixture; (b) water/glycerol: 100/0 mixture; (c) water/glycerol 70/30 and 100/0 mixtures at 30°C.

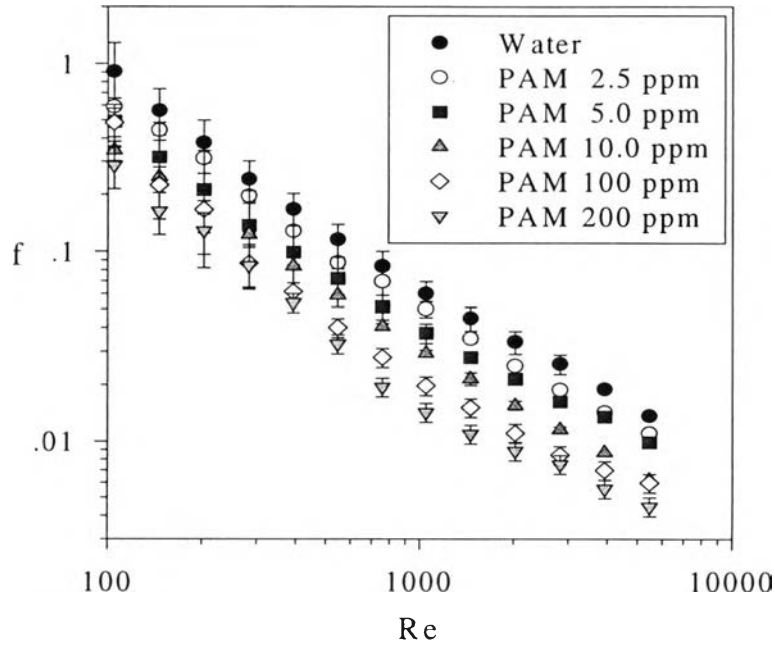

Figure 3.10 Friction factor as a function of Reynolds number for PAM-PS-02806 solutions at 30°C.

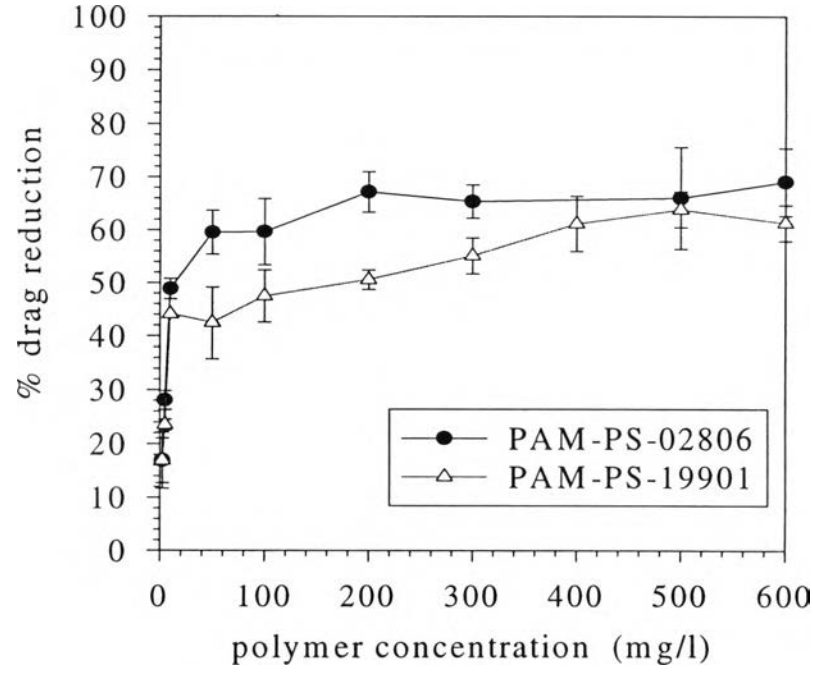

Figure 3.11 % Drag reduction as a function of polymer concentration for PAM-PS-02806 and PAM-PS-19901 solutions at Reynolds number of 5460 at 30°C.

increasing polymer concentration until reaching a particular concentration. After this point, there is a characteristic level off of the drag reduction with increasing polymer concentration. This is so called saturation phenomenon (Lumley, 1973). The saturated point for PAM-PS-19901 and PS-02806 are 61.8% at 400 mg/l and 65.3% at 200 mg/l, respectively. This can be explained by a model in figure 3.12.

Figure 3.12 shows the physical picture of polymeric molecules in the turbulent domain. Below the saturated point, when polymer concentration increases, number of chains that interfere with the truncation of small eddies increases and therefore drag reduction also increases. Near the saturated point, when polymer concentration increases, not only there is an increase in number of chains but also a decrease in end-to-end distance occurs due to the crowding effect, resulting in a decrease in the elasticity of polymer chains (de Gennes, 1990). Above the saturated concentration, there is no change in % turbulent drag reduction because an increase in number of chains is compensated by a decrease in elasticity of the chains. It may also be seen from figure 3.11 that the higher the average molecular weight, the more effective a given polymer is for turbulent drag reduction. As the average molecular weight is increased from 4.95×10^5 for PAM-PS-19901 to 2.15×10^6 for PAM-PS-02806 (Table3.3), the solution concentration required to achieve about 62% drag reduction is reduced from 400 to 100 mg/l.

3.2.2 Effect of Molecular Weight. The effect of molecular weight was studied by using several polymer samples with a fixed concentration and identical chemical structure but different molecular weights.

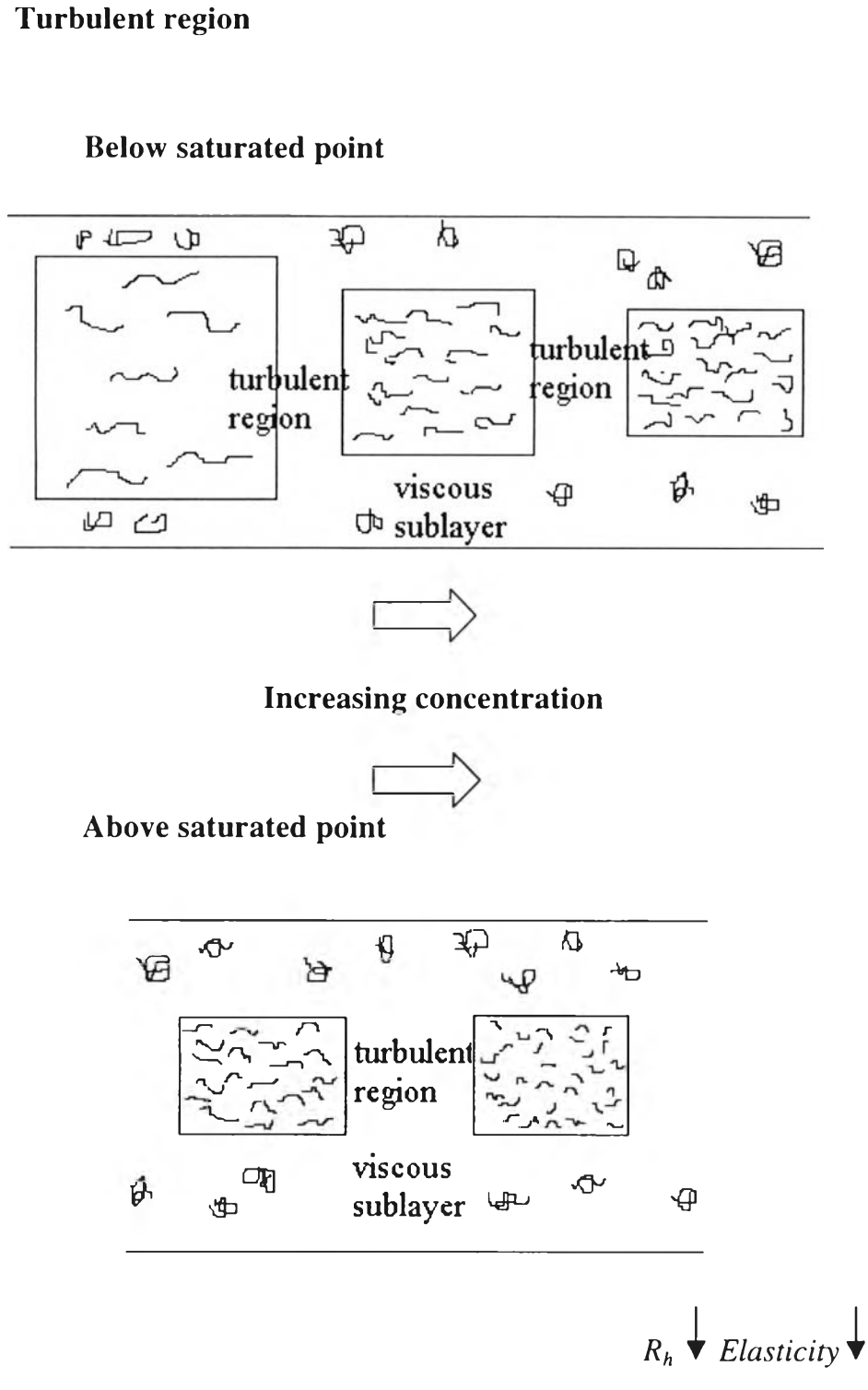

Figure 3.12 Physical picture of polymeric molecules in the turbulent region.

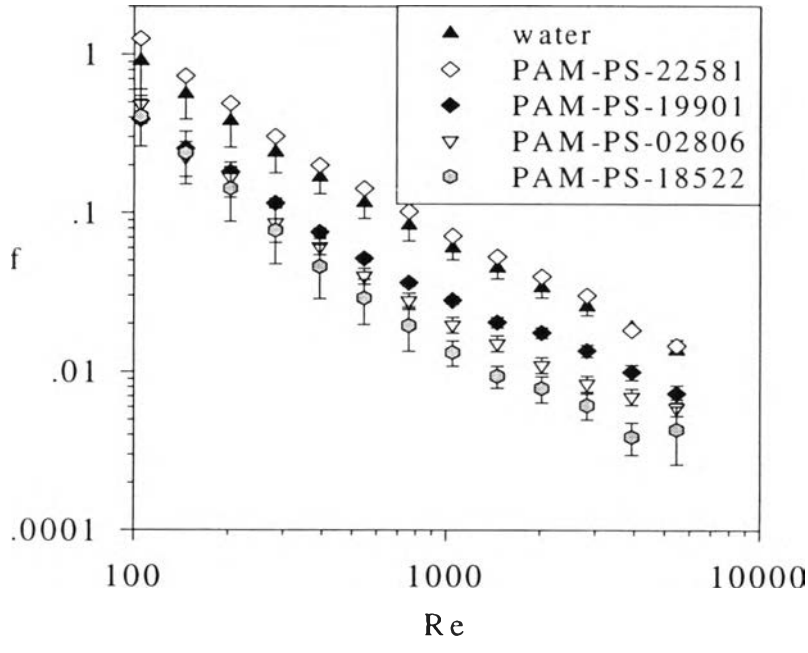

Figure 3.13 Friction factor as a function of Reynolds number for PAM-PS-22581, -PS-19901, -PS-02806, and -PS-18522 solutions at 30°C.

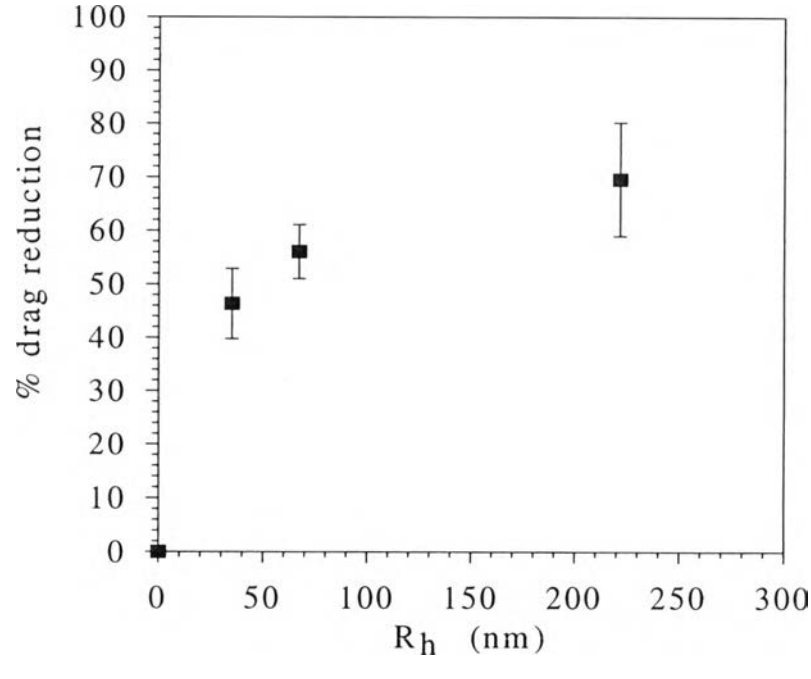

Figure 3.14 % Drag reduction as a function of polymer hydrodynamic radius for 100 mg/l PAM-PS-22581,-PS-19901,-PS-02806,-PS-18522 solutions at Reynolds number of 5460 at 30°C.

Figure 3.13 shows a plot between friction factor and Reynolds number for 100 mg/l PAM-PS-22581, PS-19901, PS-02806 and 18522 solutions at 30°C.

The measured molecular weights are tabulated in Table 3.3. When polymer concentration is held constant, friction factor decreases with increasing molecular weight. The measured friction factors are lowest for the highest molecular weight PAM-PS-18522 sample and highest for the lowest molecular weight PAM-PS-22581. Turbulent drag reduction did not occur when we added PAM-PS-22581 sample with the molecular weight of $1x10^4$. In general, the previously published result (Hoyt,1986) indicated that any soluble polymers must be of a sufficiently high molecular weight (greater than $1x10^5$) for drag reduction to occur. This is because long polymer molecules are only ones capable of acting as a network to interact with turbulent eddies, and to suppress fluctuations. Thus the longer the molecule, the more efficiency for interaction with fluctuating velocities and large scale motion.

Figure 3.14 shows % turbulent drag reduction as a function of polymer hydrodynamic radius at Reynolds number of 5460 for different molecular weight solutions of PAM at 30°C. % Turbulent drag reduction increases with increasing polymer hydrodynamic radius. We may say that the hydrodynamic radius is one of important parameters for reducing drag. However, it is unclear that whether degree of polymerization, *N*, or hydrodynamic radius, R_h can provide the best correlation. Molecular weight distribution which is not addressed in this study, may also play an important role in these relationship (Hunston and Reishman, 1975).

3.2.3 Effect of Salt Concentration. The relationship between polymer hydrodynamic radius and turbulent drag reduction was further examined in the

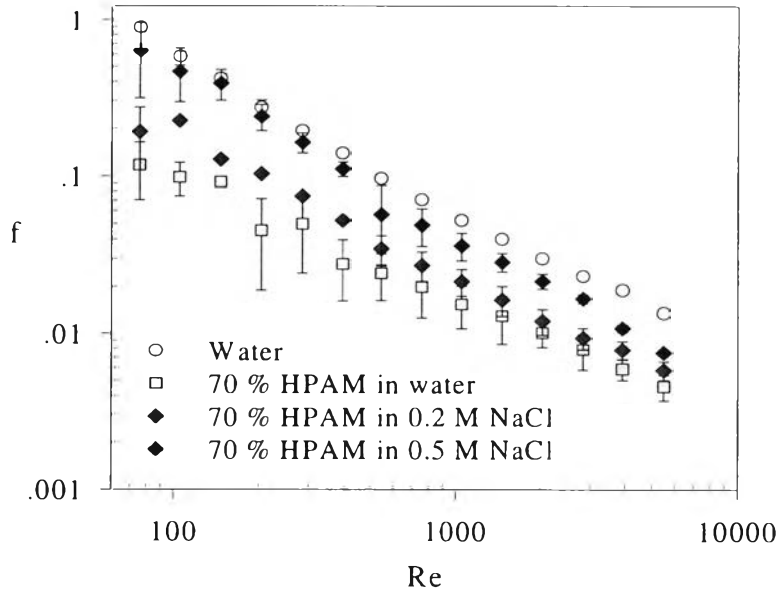

Figure 3.15 Friction factor as a function of Reynolds number for 100 mg/l 70%HPAM-SPP-377 at various NaCl concentrations from 0 M to 0.5 M at 30°C.

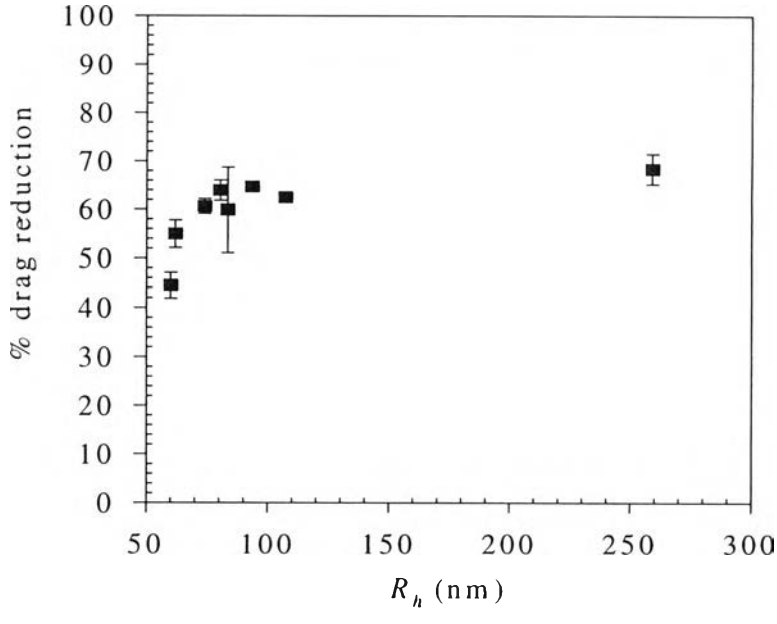

Figure 3.16 % Drag reduction as a function of polymer hydrodynamic radius for 100 mg/l 70%HPAM-SPP-377 at various NaCl concentrations from 0 M to 0.5 M at Reynolds number of 5460 at 30°C.

study of drag reduction behavior of polyelectrolyte with a fixed molecular weight and polymer concentration in a solvent by varying ionic strengths. In this study, coil volume was altered by changing solvent quality while polymer molecular weight remained unchanged.

Figure 3.15 is a plot of friction factor as a function of Reynolds number for 100 mg/l of 70% HPAM-377 in sterile water, in 0.02 M NaCl, and in 0.5 M NaCl at 30°C. Friction reduction is the greatest in sterile water in which polymer hydrodynamic radius would be expected to be the largest and the least in 0.5 M NaCl solution in which polymer chain should be collapsed due to the screening effect. This indicates that at fixed polymer concentration and molecular weight, turbulent drag reduction can be correlated with increasing polymer hydrodynamic radius through the change in solvent quality.

Figure 3.16 shows % turbulent drag reduction as a function of polymer hydrodynamic radius for 100 mg/l solution of a polyelectrolyte sample (70%HPAM-377) in sterile water and in various NaCl solutions at Reynolds number of 5460 at 30°C. The concentration of NaCl was varied from 0.005 to 0.5 M. The % turbulent drag reduction slightly increases with increasing polymer hydrodynamic radius. This may be due to chain rigidity presented in these polyelectrolytes with decreasing salt concentration. This agrees with the previous result (Zakin et al., 1980) which proposed that relative drag reduction effectiveness decreased with rigidity.

3.3 Scaling Analysis

From section 3.2, polymer hydrodynamic radius and polymer concentration are thought to be important parameters in drag reduction phenomenon. So in this section, the correlation between these parameters and

drag reduction parameters in term of the dissipative eddy sizes, l_d and the specific dissipative eddy sizes, l_d/l_{do}-1 are tested by scaling relation:

$$l_d \propto R_h^n c_p^m \quad \text{or} \quad \propto \phi^o c_p^m \quad \text{or} \quad N^t c_p^m \tag{3.5}$$

$$l_d/l_{do}\text{-}1 \propto R_h^r c_p^s \quad \text{or} \quad \propto \phi^q c_p^s, \tag{3.6}$$

l_d is simply a set of dissipative eddies whose the smallest scale, Kolmogorov microscale, l_k is defined by (Tennekes and Lumley, 1972):

$$l_k = \frac{\nu^{3/4}}{\varepsilon^{1/4}}, \tag{3.7}$$

where ν is kinematic viscosity and ε is energy dissipation rate per unit mass which equals to $\frac{u_*^{3/4}}{4\nu}$ at the maximum of dissipation spectrum, then:

$$l_k = \frac{\sqrt{2}\nu}{u_*}, \tag{3.8}$$

where u_* is the friction velocity which is defined as $u_* = (\tau_w / \rho)^{1/2}$. l_d is proportional to or scales with l_k, therefore we will determine l_d through the relation: $l_d = \frac{\sqrt{2}\nu}{u_*}$.

Figure 3.17 (a) shows a plot of l_d versus polymer hydrodynamic radius of 100 mg/l PAM-PS-19901, PS-02806 and PS-18522 solutions and 100 mg/l 70% HPAM-SPP-377 solutions at various salt concentrations in logarithmic scale. The data were fitted to a linear form. The scaling exponents, n obtained from the logarithmic slope are 0.56 and 0.62 for varying NaCl concentration and equal to 0.62 and 0.77 for varying molecular weight at Reynolds numbers of 5460 and 1050, respectively. They are slightly different for each particular polymer type.

Figure 3.17 (b) shows l_d/l_{do}-1 as a function of polymer hydrodynamic radius for 100 mg/l PAM-PS-19901, PS-02806 and PS-18522 solutions and 100 mg/l 70%HPAM-SPP-377 solutions at various salt concentrations. The scaling exponents, r, are 1.15 and 1.45 for the various NaCl concentrations and equal to 1.08 and 1.09 for the various molecular weights at the Reynolds numbers of 5460 and 1050, respectively.

Figure 3.18 (a) is a plot between l_d and polymer volume fraction, ϕ, for 100 mg/l PAM-PS-19901, PS-02806 and PS-18522 solutions and 100 mg/l 70%HPAM-SPP-377 solutions at various salt concentrations. The scaling exponents, o, obtained from the logarithmic slope are 0.19 and 0.21 for the various NaCl concentrations and equal to 0.43 and 0.50 for the various molecular weights at Reynolds numbers of 5460 and 1050, respectively.

Figure 3.18 (b) shows a plot between l_d/l_{do}-1 versus polymer volume fraction, ϕ, for 100 mg/l PAM-PS-19901, PS-02806 and PS-18522 and 100 mg/l 70%HPAM-SPP-377 at various salt concentrations. The scaling exponents, q, obtained from the logarithmic slope are 0.36 and 0.36 for the various NaCl concentrations and equal to 0.92 and 1.06 for the various molecular weights at Reynolds numbers of 5460 and 1050, respectively.

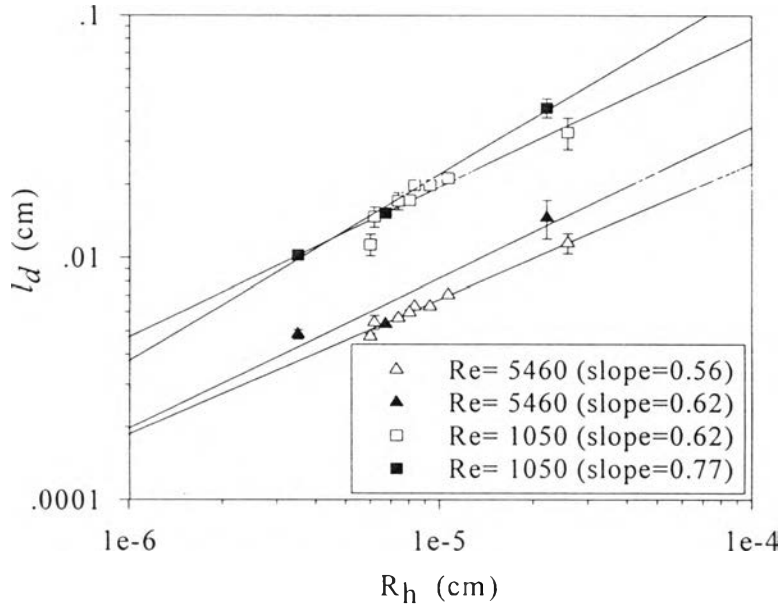

Figure 3.17 (a) l_d as a function of polymer hydrodynamic radius for 100 mg/l PAM-(PS-19901, PS-02806 and PS-18522) solutions, ■ ▲, and 100 mg/l 70%HPAM-SPP-377 at various salt concentrations, □ △, at 30°C.

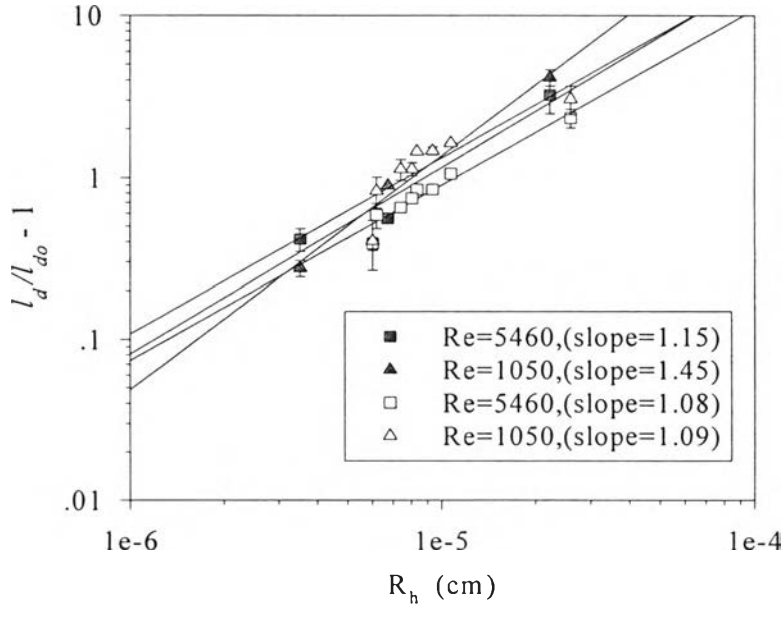

Figure 3.17 (b) l_d/l_{do} – 1 as a function of polymer hydrodynamic radius for 100 mg/l PAM -PS-19901, -PS-02806 and -PS-18522 solutions, ■ ▲, and 100 mg/l 70%HPAM-SPP-377 at various salt concentrations, □ △, at 30°C.

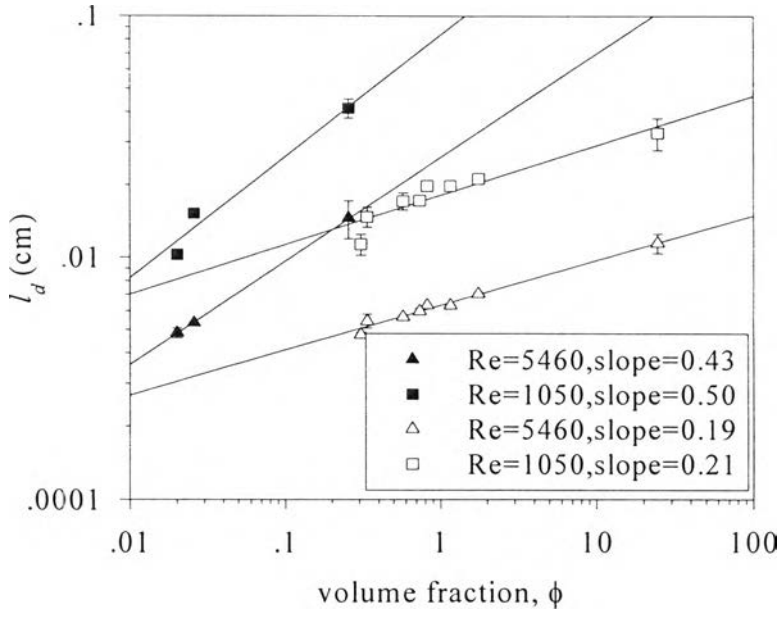

Figure 3.18 (a) l_d as a function of polymer volume fraction for 100 mg/l PAM-(PS-19901, PS-02806 and PS-18522) solutions,■ ▲ , and 100 mg/l 70%HPAM-SPP-377 at various salt concentrations,□ △ , at 30°C.

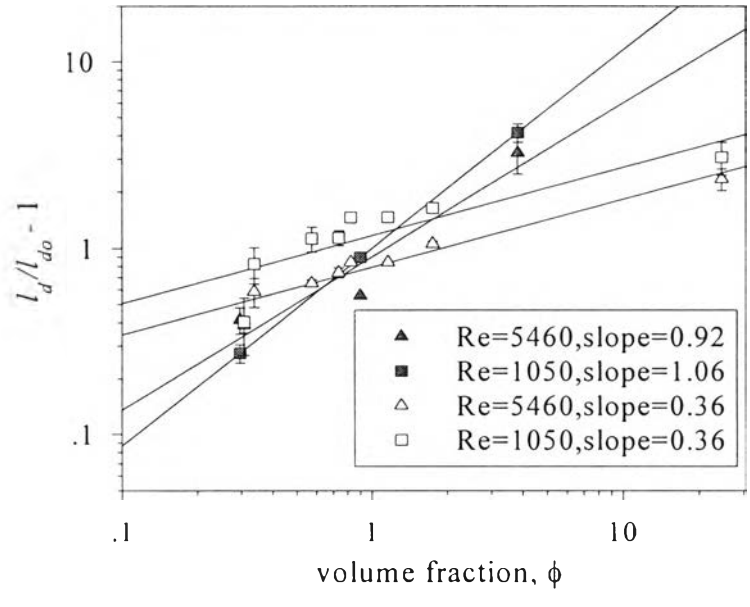

Figure 3.18 (b) $l_d/l_{do} - 1$ as a function of polymer volume fraction for 100 mg/l PAM-(PS-19901, PS-02806 and PS-18522) solutions,■ ▲, and 100 mg/l 70%HPAM-SPP-377 at various salt concentrations,□ △, at 30°C.

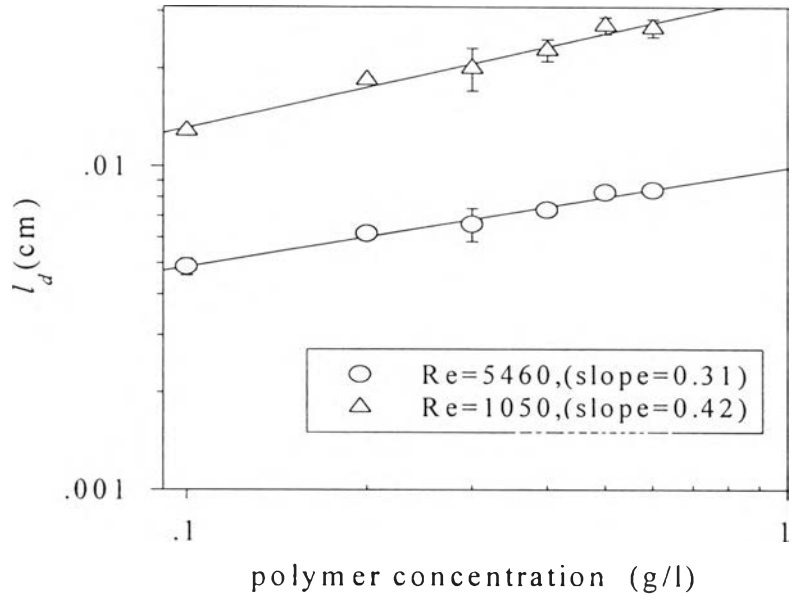

Figure 3.19 (a) l_d as a function of polymer concentration for PAM-PS-02806 solutions at 30°C.

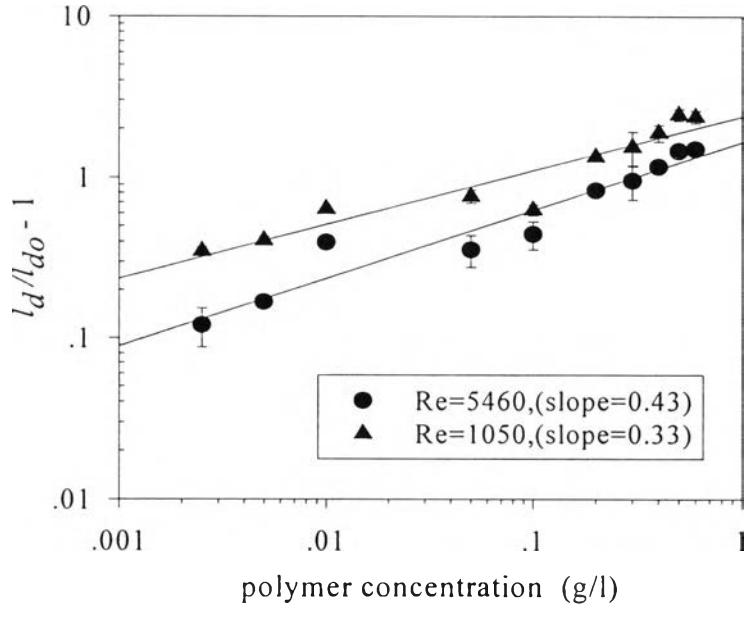

Figure 3.19 (b) $l_d/l_{do} - 1$ as a function of polymer concentration for PAM-PS-02806 solutions at 30°C.

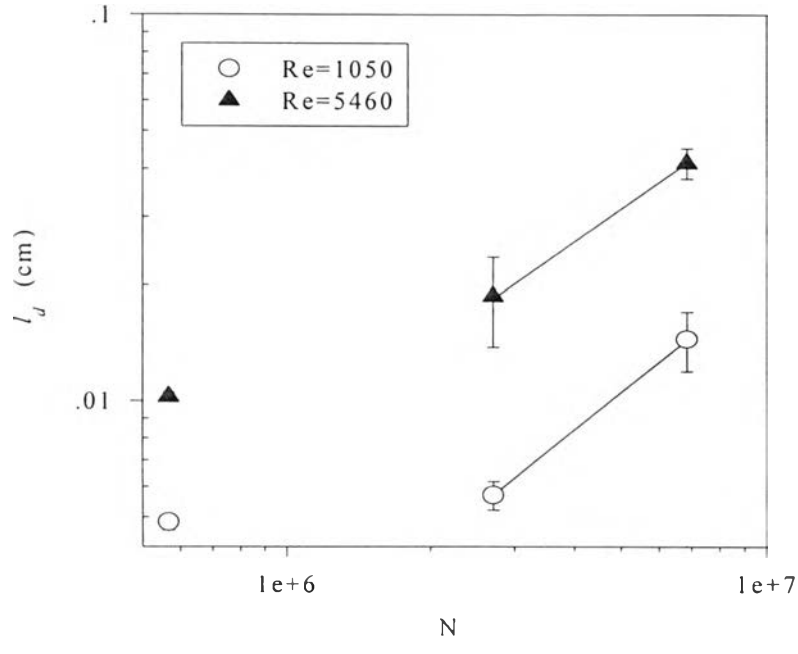

Figure 3.20 l_d as a function of N of PAM at 30°C.

Figure 3.19 (b) is a plot between l_d/l_{do}-1 versus polymer concentration of PAM-PS-02806. l_d/l_{do}-1 also increases with increasing polymer concentration. The scaling exponents, s, obtained from logarithmic slope are 0.43 and 0.33 for Reynolds numbers of 5460 and 1050, respectively.

Figure 3.20 is a plot between l_d versus degree of polymerization. l_d also increases with increasing degree of polymerization. the scaling exponents, t, obtained from logarithmic slope are 0.87 and 1.00, respectively.

The dependence of scaling exponents of dissipative eddy sizes and specific dissipative eddy sizes on polymer hydrodynamic radius, polymer volume fraction polymer concentration and degree of polymerization are tabulated in Table 3.7.

Table 3.7 Scaling exponents of l_d , l_d/l_{do}-1 on polymer hydrodynamic radius, polymer volume fraction and polymer concentration.

Parameters		Concentration		Molecular weight		Salt concentration	
	Re	l_d	l_d/l_{do}-1	l_d	l_d/l_{do}-1	l_d	l_d/l_{do}-1
R_h	5460	-	-	0.62	1.08	0.56	1.15
	1050	-	-	0.77	1.09	0.62	1.45
ϕ	5460	-	-	0.43	0.92	0.19	0.36
	1050	-	-	0.50	1.06	0.21	0.36
c_p	5460	0.31	0.43	-	-	-	-
	1050	0.42	0.33	-	-	-	-
N	5460	-	-	1.00	-	-	-
	1050	-	-	0.87	-	-	-